Structure of the $11/2^-$ isomeric state in ^{133}La

Md. S. R. Laskar,[1] R. Palit,[1] S. N. Mishra,[1,2] N. Shimizu,[3] Y. Utsuno,[4,3] E. Ideguchi,[5] U. Garg,[6] S. Biswas,[1] F. S. Babra,[1] R. Gala,[1] C. S. Palshetkar,[1] and Z. Naik[7]

[1]*Department of Nuclear and Atomic Physics, Tata Institute of Fundamental Research, Mumbai 400005, India*
[2]*Indian Institute of Science Education and Research, Berhampur-760010, India*
[3]*Center for Nuclear Study, The University of Tokyo, Hongo, Bunkyo-ku, Tokyo 113-0033, Japan*
[4]*Advanced Science Research Center, Japan Atomic Energy Agency, Tokai, Ibaraki 319-1195, Japan*
[5]*Research Center for Nuclear Physics (RCNP), Osaka University, Ibaraki, Osaka 567-0047, Japan*
[6]*Physics Department, University of Notre Dame, Notre Dame, Indiana 46556, USA*
[7]*Physics Department, Sambalpur University, Sambalpur-768019, India*

(Received 5 January 2020; accepted 9 March 2020; published 31 March 2020)

We report measurement of the g-factor for the $11/2^-$ isomeric state at 535 keV in ^{133}La, employing the time differential perturbed angular distribution technique (TDPAD). This isomer was populated in the reaction ^{126}Te(^{11}B, $4n$) ^{133}La at beam energy of 52 MeV. From the observed nuclear spin precession, analysed through combined, magnetic dipole and electric quadrupole hyperfine interactions, we obtain the g factor for the $11/2^-$ state as $g = 1.16 \pm 0.07$. In addition, this analysis provides the spectroscopic quadrupole moment $|Q| = 1.71 \pm 0.34$ b, yielding the deformation parameter $\beta = 0.28 \pm 0.10$. Further, we have performed theoretical calculations using the large-scale shell model and the Monte Carlo shell model. The results successfully describe the low-lying levels and the band structures of ^{133}La, and the calculated g factor compares well with the values obtained from our experiment. The dominant configuration of $11/2^-$ isomeric state in ^{133}La is inferred to be $\pi(h_{11/2}) \otimes {}^{132}\mathrm{Ba}(0^+)$.

DOI: 10.1103/PhysRevC.101.034315

I. INTRODUCTION

The level structures of nuclei evolve from single-particle to collective nature, as one goes away from the $Z = 50$ and $N = 82$ shell gaps. The transitional nuclei around $A \approx 135$ with $Z > 50$ and $N < 82$ lie between the spherical and deformed regions and show complex and rich level structures due to interplay for single-particle and collective excitation modes [1–3]. Occupation of high-j orbitals for protons and neutrons plays a crucial role for various structure phenomena for nuclei in this region, such as signature splitting, signature inversion, magnetic rotation, wobbling motion, chiral rotation, and high-spin isomers. With the advancement of large-scale shell-model (LSSM) calculations [4], it is now possible to make microscopic analysis on the high-spin structures of these nuclei, as well as the configuration of the isomers. The electromagnetic moment measurements of the isomers in these nuclei are of particular interest, as they provide a stringent test of the LSSM calculations. Recently, the isomers in ^{135,136}La isotopes have attracted lot of attention [3,5,6]. As a part of a systematic study of the isomers in this region, we have performed experiments to measure the g factor of the well-known $11/2^-$ isomer in ^{133}La isotope and compare the results with the LSSM calculations. In the present investigation, combined (the magnetic and electric) perturbations of the angular distribution pattern of the deexciting γ rays from the respective isomeric states has been exploited for the determination of the g factor and quadrupole moment of $11/2^-$ isomeric state at 535-keV in ^{133}La [7–10], using time differential perturbed angular distribution technique (TDPAD). There are only two previous moment measurements for the g factor of the 535 keV state in odd mass La nuclei. Gerschel *et al.* assigned the 535-keV level as $3/2^-$ state and reported $g = 2.2$ [11]. Assuming $I^\pi = 11/2^-$, the g factor would be 0.6. They employed the 510-keV-58-keV angular correlation to extract the g factor. In the recent compilation of nuclear moments [12], the g factor of the 535-keV isomer in ^{133}La has been listed as 1.37 ± 0.08, with an assigned $I^\pi = 11/2^-$. The details of the original measurement can be found in Ref. [13], where the g factor of the 535-keV state was measured using 477-keV, −58-keV, and 510-keV−58-keV angular correlation from the decay data of ^{133}Ce. However, certain experimental details about the detectors and the observed Larmor frequency along with spin-rotation spectrum were not presented in Ref. [13]. Furthermore, Gerschel *et al.* [14] reported the quadrupole moment of the 535-keV state in ^{133}La to be $Q = 1.6 \pm 0.2$ b. On the other hand, for the same state in ^{133}La, the measurement of Klemme *et al.* [15] reported the quadrupole moment to be $Q = 0.35 \pm 0.03$ b. Both these quadrupole measurements assumed $I^\pi = 3/2^-$ for the 535-keV state. Considering that the quadrupole interaction frequency $\omega_Q = \frac{eQV_{zz}}{(4I(2I-1))\hbar}$, if one considers the $I^\pi = 11/2^-$ for the 535-keV state, for the same value of ω_Q, the quadrupole moment would be 18 times of the values reported in Refs. [14,15]. Clearly, the electromagnetic moments reported from previous experiments are quite

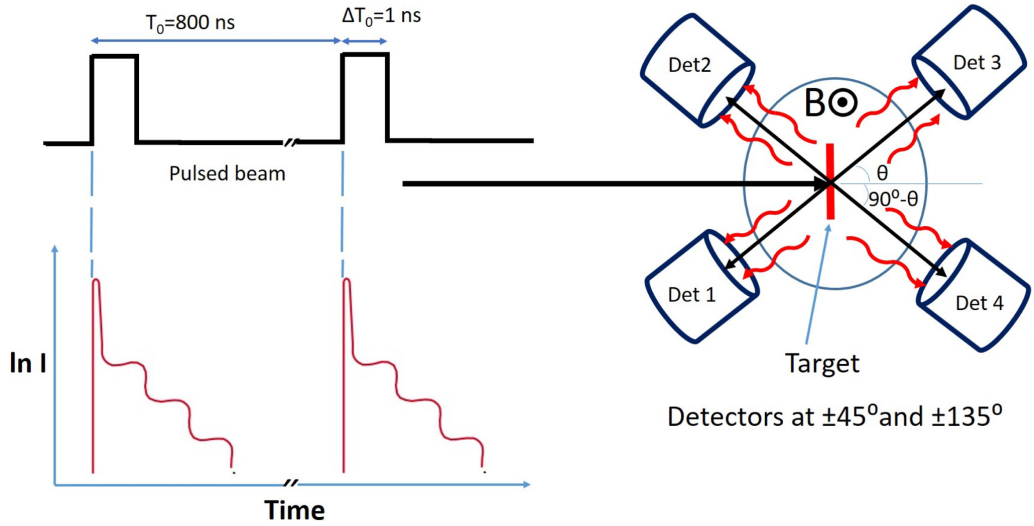

FIG. 1. Schematic drawing of the experimental arrangement of the TDPAD setup.

disparate. These values are also in contrast to the concept of decoupling limit or rotational alignment for the explanation of the decoupled bands in the odd-mass $^{125-139}$La nuclei [16–18]. It is also interesting to compare the measured g factor for $11/2^-$ state in ^{133}La ($N = 76$) with that of ^{129}Cs ($N = 74$) [19] and ^{141}Pr ($N = 82$) [20]. The tabulated value of g factor for the $11/2^-$ state in ^{133}La [12] is closer to the Schmidt value and the value in ^{141}Pr, compared to that in ^{129}Cs [19]. As $\Delta I = 2$ bands have been observed on the $h_{11/2}$ quasiproton states in ^{129}Cs and ^{133}La isotopes, one expects the g factor of $11/2^-$ state in ^{133}La to be similar to that of ^{129}Cs due to their modestly deformed even-even cores, rather than that of ^{141}Pr which has a spherical core. In view of the above-mentioned discrepancies in the g factor, it is important to carry out accurate measurements of electromagnetic moments for the $11/2^-$ isomeric state in ^{133}La. In this work, we present precision measurement of g factor and quadrupole moment for the 535-keV, $11/2^-$ isomer in ^{133}La using time differential perturbed angular distribution (TDPAD) technique. The measured g factor and the quadrupole moment have been compared with the results obtained from theoretical calculations performed using the LSSM.

II. EXPERIMENTAL DETAILS

The $11/2^-$ isomeric level at 535 keV in ^{133}La was populated through the reaction ^{126}Te(^{11}B, $4n$) ^{133}La at 52-MeV beam energy. The ^{11}B beam having a pulse width of 1 ns and repetition period of 800 ns, was provided by the BARC-TIFR Pelletron Linac Facility at TIFR, Mumbai. An isotopically enriched 1.2 mg/cm^2-thick ^{126}Te was evaporated on to a 9.9 mg/cm^2-thick Au backing. From simple kinematic considerations, the recoil energy of the La nuclei was estimated to be ≈4.17 MeV. Using a Monte Carlo method based on statistical model SRIM [21,22], we have found that the ^{133}La nuclei stop within the Te target, with only a negligible fraction penetrating in to the Au backing constituted the target. The experiments were performed in the presence of a magnetic field $B_{\rm ext} = 2$ T, applied perpendicular to the beam-detector plane. The magnetic field was produced using a split coil superconducting magnet having field stability of better than 0.1% and uniformity of 0.5% over a spherical volume of ≈1 cm^3. The field direction was reversed in every 6 hours. The schematic diagram of the experimental arrangement is shown in Fig. 1. This setup has been regularly used to investigate magnetic properties of materials and studies of hyperfine interactions using TDPAD technique [6,23–25].

The delayed γ rays from the 535-keV isomer were measured by large volume (≈143 cm^3) HPGe detectors with relative efficiency of 30% with respect to a 3 × 3 inch NaI(Tl) scintillation detector. The detectors were placed at a distance of 11 cm from the target center at angles ±45° and ±135° with respect to the beam direction. The time resolution of the detectors was measured to be 5 ns at γ energy of 1332 keV of the standard ^{60}Co radioactive source. The time signal from the HPGe detector was used to start the time to amplitude converter (TAC), which was stopped by the primary RF signal of the buncher. The data were collected in LIST mode with eight parameters for energy and time signals for four detectors. In the off-line analysis, two-dimensional spectra with energy versus time were constructed for each detector. The lifetime spectra for the γ rays decaying from the isomeric state were generated by taking energy-gated time projections. Normalized counts for each detector $N(\theta, t)$ were used to construct the spin rotation spectra defined as

$$R(t) = \frac{[N \uparrow (\theta, t) - N \downarrow (\theta, t)]}{[N \uparrow (\theta, t) + N \downarrow (\theta, t)]}. \quad (1)$$

The form of $R(t)$ varies depending on the geometry of experimental setup and hyperfine interactions present, e.g., due to a magnetic dipole, an electric quadrupole, or both [26–28]. For a pure magnetic dipole interaction, the spin rotation function for the experimental geometry used here can be expressed as

$$R(t) = A_2 G_2(t) = -\tfrac{3}{4} A_2 \sin(2\omega_L t - \phi)\exp(-\lambda t), \quad (2)$$

where A_2 is the amplitude, G_2(t) is the perturbation function due to magnetic hyperfine interaction with Larmor frequency

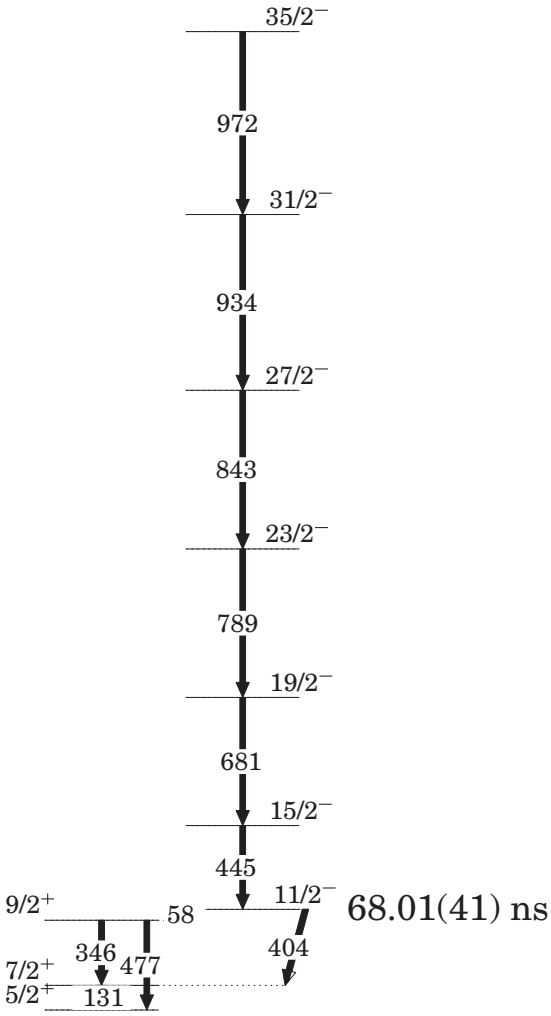

FIG. 2. Partial level scheme of ^{133}La showing the isomer at 535 keV (adopted from Ref. [10]).

ω_L, and λ is a damping factor signifying the loss of nuclear spin alignment arising from dynamic fluctuations of electronic spin and/or inhomogeneous distribution in local environment. ϕ denotes a phase angle due to finite bending of the incoming beam due to applied magnetic field. In the case of a pure electric quadrupole interaction, the perturbation to the angular distribution function $G_2(t)$ is expressed as [29,30]:

$$G_2(t) = \left[S_{20}(\eta) + \sum_{n=1}^{3} S_{2n}(\eta)\cos(\omega_n t) g'(\omega_n \delta t) \right] \exp(-\lambda t). \tag{3}$$

In presence of combined interactions, the perturbation function is more complex, having the general form [31,32]:

$$G_2(t) = \left[a_0(\eta, y, \beta') + \sum_{n} a_n(\eta, y, \beta') cos(\omega_0 t) g'(\omega_0 \delta t) \right], \tag{4}$$

where S_{20} is a constant known as the hard core contribution, S_{2n} are the amplitudes of the primary quadrupole interaction frequencies ω_n, η is the asymmetry parameter of the

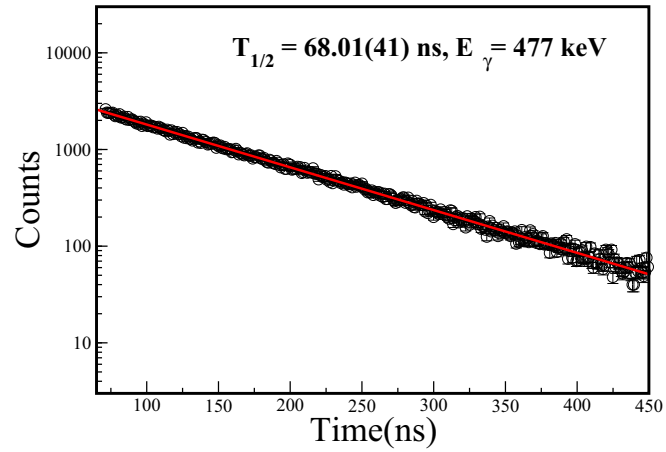

FIG. 3. Lifetime decay spectrum obtained with energy gate on the 477 keV γ line.

electric field gradient (EFG) tensor usually expressed as $\eta = \frac{V_{yy}-V_{xx}}{V_{zz}}$ with $V_{zz} > V_{yy} > V_{xx}$ and $0 \leqslant \eta \leqslant 1$. The number of frequency components $\omega_n = b_{2n}(\eta)\omega_0$ and their amplitudes a_n depend on the relative strength of the magnetic and quadrupole interactions defined by the ratio $y = \omega_L/\omega_Q$ and the angle β' between the magnetic field and the EFG axis; $\omega_0 = 3\omega_Q$ for odd spin and $\omega_0 = 6\omega_Q$ for even spin. The coefficient is $b_{2n} = n$ for $\eta = 0$ [33]. $g'(\omega_n t\delta)$ describes the damping due to the static distribution in ω_n arising from the random inhomogeneities in the local environment of the probe nuclei, which, conventionally, is assumed to be either Lorentzian or Gaussian with δ being the distribution width. $G_2(t)$ for combined interactions are generally solved numerically by varying y and β' [34].

III. RESULTS AND DISCUSSION

A. Experimental results

The partial levels scheme of ^{133}La relevant for the current study is shown in Fig. 2. Figure 3 shows the lifetime spectrum fitted with an exponential decay curve with energy gate on the 477-keV γ line to give a lifetime ($T_{1/2}$) of 68.01 ± 0.41 ns, with the quoted uncertainty being only statistical; this value is within the range [7,10].

The energy-gated time spectrum generated with the 477-keV transition was used to construct the spin rotation spectra $R(t)$ displayed in Fig. 4. The observed spectrum shows a large amplitude, which suggests that most of the ^{133}La probe nuclei come to rest at a regular lattice sites in the Te host, most likely to be substitutional.

Let us first consider that the ^{133}La nuclei stopped in Te host experience pure magnetic interaction. A fit of our experimentally observed $R(t)$ spectra to Eq. (2) yielded the value for $\omega_L = 114.2 \pm 5.0$ Mrad/s, $\phi \approx 16^\circ \pm 5^\circ$ and $\lambda = 13.5 \pm 5.5$ MHz. Using the expression $\hbar\omega_L = g_N \mu_N B_{\text{ext}}$, and neglecting paramagnetic and/or diamagnetic correction factors, we obtain the g factor as 1.19 ± 0.06. Note, however, that the spin-rotation spectrum shows strong damping (see Fig. 4) with a very large value of λ. One factor leading to a strong

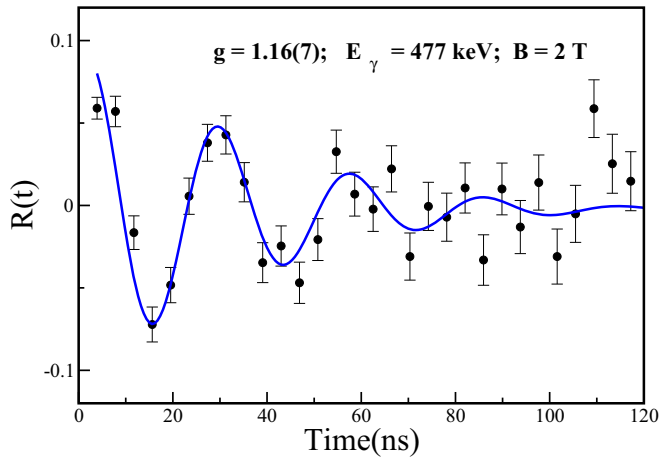

FIG. 4. Spin rotation spectrum of $11/2^-$ isomeric state of ^{133}La with $B_{\rm ext} = 2$ T.

damping in the $R(t)$ spectra is the distribution in frequency, caused by beam induced radiation damage in the Te host. It is worthwhile to note, however, that spin rotation spectra of ^{135}La [35] implanted into an Fe host, measured under conditions similar to the present study, did not show much damping. This suggests that beam induced radiation damage does not have significant contribution to the damping observed in the $R(t)$ spectra of ^{133}La. Note that in the present experiment, the ^{133}La nuclei come to rest within the ^{126}Te target matrix. Te metal has hexagonal close-packed (hcp) crystal structure, which will produce nonzero electric field gradient at the probe site. Thus, the ^{133}La nuclei in Te host will experience the combined influence of the magnetic dipole and electric quadrupole interaction [36]. We therefore refined our data analysis by considering the perturbation function due to the combined interaction. A fit of the $R(t)$ spectrum using Eq. (4) yielded $\omega_L = 111.4 \pm 6.7$ Mrad/s and $\omega_Q = 8.0 \pm 1.0$ Mrad/s. From the ω_L value, we extract $g = 1.16 \pm 0.07$, which is close to the value estimated with pure magnetic interaction. We note that the Schmidt value for the single-particle g factor for proton in $h_{11/2}$ configuration is estimated to be $g_{\rm schmidt} = 1.42$; the experimental value is, thus, quenched from the Schmidt value by 18%.

To determine the spectroscopic quadrupole moment $|Q|$ from ω_Q, one has to know the value of the EFG at a lanthanum nucleus site in a ^{126}Te crystal. The EFG is a traceless second rank tensor defined by the second derivative (in Cartesian coordinates) of the Coulomb potential at the nuclear position. The Coulomb potential is calculated from the self-consistently obtained total charge distribution, by solving the Poisson equation. The EFG can be easily calculated, once the Coulomb potential is known. The field gradient tensor is diagonalized and principal components are rearranged such that $|V_{xx}| \leqslant |V_{yy}| \leqslant |V_{zz}|$; the EFG is conventionally defined by V_{zz}, while $(V_{xx} - V_{yy})/V_{zz}$ gives the asymmetry parameter related to the point symmetry of the atomic site. To find the EFG of a La impurity in Te host, we have performed first principle *ab initio* band structure calculations within the framework of density functional theory [37–39], using the augmented plane wave+local orbital (APW+lo) method [39–41] as implemented in the WIEN2K package [42].

The calculations were carried out using a supercell consisting of 27 ($3 \times 3 \times 3$) unit cells of the pure Te structure. One of the Te atoms within the supercell was replaced by La. The unit cell thus contains 54 (1 La +53 Te) atoms, which is representative of a dilute alloy of La_xTe_{1-x} with impurity concentration, $x = 0.0185$. All calculations were performed using the experimental lattice parameter of elemental Te ($a = 4.4572$ Å, $c = 5.9290$ Å) taken from literature [43]. In the APW+lo method, the unit cell is divided into two regions: (i) nonoverlapping muffin-tin spheres of radius R_{MT} around each atom; and (ii) the remaining interstitial region. For the wave functions inside the atomic spheres, a linear combination of radial function times spherical harmonics are used, while in the interstitial region a plane wave expansion is used. In our calculations, we have used R_{MT} values of 2.4 a.u. for La and 2.4 a.u. for Te. The maximum multipolarity l for the waves inside the atomic sphere was restricted to $l_{\rm max} = 10$. The wave functions in the interstitial region were expanded in plane waves with a cutoff of $k_{\rm max} = 7.5/R_{\rm MT}^{\rm min} = 3.125$ a.u.$^{-1}$. The charge density was Fourier expanded up to $G_{\rm max} = 16\sqrt{\rm Ry}$. For the exchange correlation potential, we used the Perdew-Burke-Ernzerhof (PBE) formalism of the generalized gradient approximation (GGA) [44]. For sampling of the Brillouin zone a dense k mesh of 256 of size $8 \times 4 \times 8$ was used. Due to lattice imperfection caused by the introduction of an impurity, the atoms at their ideal positions experience nonzero force, which was minimized by allowing the atoms to relax to new positions until the force reduced to less than 1 mRy/a.u. The self consistency of the calculations were ascertained from the energy and charge convergence criterion set to be 0.01 mRy and 0.0001, respectively.

From the calculation performed with the above-mentioned parameters, we obtained the EFG for the La impurity in Te host to be $V_{zz} = 6.7 \times 10^{17}$ V/cm^2 after considering lattice relaxation. Using this value of V_{zz}, and the expression [36], $\hbar|\omega_Q| = \frac{eQV_{zz}}{4I(2I-1)}$, we obtained the spectroscopic quadrupole moment of $11/2^-$ isomer as $|Q| = 1.71 \pm 0.34$ b. The quadrupole moment is related to the deformation parameter β through the relation

$$Q_s = \frac{3}{\sqrt{5\pi}} eZ\beta(1 + 0.16\beta)R_0^2 A^{2/3} \frac{3K^2 - I(I+1)}{(I+1)(2I+3)}, \quad (5)$$

where Z = atomic number of the nucleus, K = projection of total angular momentum or spin on symmetry axis, I nuclear spin and $R_0 = 1.21$ fm [45]. Considering $K = 1/2$ from the Nilsson diagram, we obtain the deformation parameter $\beta = 0.28 \pm 0.10$, consistent with the theoretical estimate discussed below. The uncertainties quoted in the value of the g factor and the quadrupole moment $|Q|$ are due to systematic and statistical errors. For magnetic moment, the statistical error is dominant and the systematic error owing to magnetic field stability as well as uniformity has been taken as less than 1%. The statistical error in the ω_L value obtained from the least square fit of the experimentally observed spin rotation spectra has been found to be approximately 6%. This leads to a net error budget of about 6% for the estimated g factor. For the

case of the quadrupole moment, however, the uncertainty in the calculated V_{zz} also contributes to the overall uncertainty in the Q value. In principle, the DFT method is exact and is expected to provide an accurate estimate of the electric field gradient. In practice, however, the calculated EFG may differ, depending on the choice of the exchange correlation potential—the two most commonly used potentials being the local density approximation (LDA) and generalized gradient approximation (GGA). The spread in the EFG calculated with both these potentials was found to be less than 2%. Other parameter settings in the DFT calculation like the size of the basis set determined by the choice of $K_{\max}$ and the k-mesh size has been found have little influence on the V_{zz} value. The choice of the unit cell parameter, on the other hand, has much stronger influence on the calculated V_{zz}. A small variation (2%) in the lattice parameters has been found to result in a spread of ≈10–15 % in the V_{zz} values [46]. This amount of uncertainty in the unit cell parameters is not unrealistic, considering that the calculation is performed with lattice constants measured at room temperature while, the DFT calculation represent the property at absolute zero temperature. Thus, in estimating the net error budget for the Q value we have assumed a systematic error of 15% due to the spread in V_{zz} arising from uncertainty in lattice parameters over and above the statistical error of 12.5% deduced from the fit of the experimentally observed $R(t)$ spectra.

A comparison of the experimental results with theoretical calculations would allow an examination of the nuclear structure of the $11/2^-$ isomeric state. For this we have performed theoretical calculations using LSSM.

B. Large-scale shell-model calculations

We have performed the large-scale shell-model (LSSM) calculations to investigate the level scheme and the 535-keV isomer of ^{133}La microscopically. The model space of the LSSM is taken as the $1d_{5/2}, 0g_{7/2}, 2s_{1/2}, 1d_{3/2}$, and $0h_{11/2}$ single-particle orbits both for protons and neutrons. As an effective interaction, we adopted the SNV interaction, which consists of the SNBG3 interaction for the neutron-neutron interaction [47], the N82GYM interaction for the proton-proton interaction [48], and the monopole-based universal interaction for the proton-neutron interaction [49]. The SNV interaction was proven to be successful in describing the nuclear structures of ^{135}La [6], ^{134}Ba [50], and the shell evolution of Sb isotopes [51].

Figure 5 shows the level scheme of ^{133}La obtained by the LSSM calculation. Its M-scheme dimension reaches 6.9×10^{10}, which can be handled with the shell-model code KSHELL [4] and recent supercomputers. In the preceding works [16,52], the band states built from the $11/2^-_1$ isomeric state were interpreted as the favored states of the decoupling limit of the particle-plus-rotor model [53]. The present shell-model study reproduces the experimental levels including the level spacing of the negative-parity band, while some states appear lower than the band members in the LSSM result. The $11/2^-_1$ state decays to the $7/2^+_1$ state with the $M2$ transition or to the $9/2^+_1$ state with the $E1$ transition. The experimental $M2$ transition probability is $B(M2; 11/2^- \to 7/2^+) = 3.1 \pm$

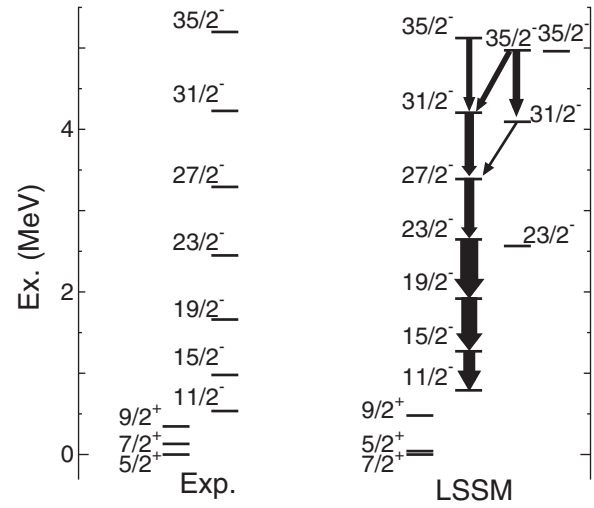

FIG. 5. Level schemes of ^{133}La by the experiments (left) and by the present LSSM calculation (right). The arrows denote the $B(E2)$ transition between the negative parity states, and their widths are proportional to the $B(E2)$ strengths with with the effective charges $(e_p, e_n) = (1.6, 0.8)e$.

0.3 $\mu_N^2 \mathrm{fm}^2$ [54], and shows reasonable agreement with the LSSM value, 6.6 $\mu_N^2 \mathrm{fm}^2$. In the LSSM, the spin part of the $M2$ transition is quenched by the factor 0.4, which is determined to reproduce the experimental $M2$ values of the Sn isotopes and $N = 82$ isotones [54]. The $E1$ transition probability cannot be obtained theoretically in the present LSSM model space.

Our measured value of the g factor of the $11/2^-_1$ state is 1.16 ± 0.07, which is compared with the LSSM results to find out the mixing of different configurations for the $11/2^-$ isomer. The calculated g factor is 1.16 with spin g factor quenched 0.64 for protons and 0.74 for neutrons [6], showing good agreement with the experimental one. This isomeric state is considered to be the band head of the favored band of the decoupling limit [16], and its configuration is $\pi(h_{11/2}) \otimes {}^{132}\mathrm{Ba}(0^+)$. Thus, its wave function can be approximated as $c^\dagger_{\pi 0h_{11/2}} |{}^{132}\mathrm{Ba}, 0^+_1\rangle$ where $c^\dagger_{\pi 0h_{11/2}}$ and $|{}^{132}\mathrm{Ba}, 0^+_1\rangle$ denote the creation operator of the proton $h_{11/2}$ orbit and the ground-state wave function of ^{132}Ba provided by the LSSM calculations, respectively. The g factor of this simple wave function without any mixing of other configurations in this state is obtained as 1.23, which is close to the experimental value and supports the present interpretation.

The spectroscopic quadrupole moments and g factors of the $11/2^-_1$ states of La isotopes are shown in Table I. Those of the ^{135,137,139}La are evaluated by the LSSM using the same Hamiltonian without any truncation with the effective charges $(e_p, e_n) = (1.6, 0.8)e$. The quadrupole moment of ^{139}La ($N = 82$) is rather small and it increases gradually as the neutron number decreases and the quadrupole collectivity increases. The LSSM quadrupole moment of ^{133}La is obtained as $Q = -1.25$ b in comparison with the experimental value, $|Q| = 1.71 \pm 0.34$ b. On the other hand, the g factors of the isotopes are rather constant indicating a proton $h_{11/2}$ configuration.

TABLE I. g factors, spectroscopic quadrupole moments, and single-particle spectroscopic factor C^2S of the $11/2^-_1$ states of La isotopes obtained by the LSSM calculations. The values obtained by the present experiment are shown in the rightmost column. Note that the experimental Q moment of ^{133}La is obtained as the absolute value. The C^2S is obtained by the proton $h_{11/2}$ attached to the ground state of the neighboring Ba isotopes.

	LSSM ^{139}La	^{137}La	^{135}La	^{133}La	Expt. ^{133}La
g factor	1.23	1.20	1.18	1.16	1.16(7)
Q moment (b)	−0.49	−0.80	−1.00	−1.25	1.71(34)
$C^2S(\pi h_{11/2})$	0.89	0.73	0.68	0.60	

Table I also shows the single-particle spectroscopic factor C^2S of the proton $h_{11/2}$ orbit with the ground states of the corresponding Ba isotopes. As the neutron number increases the C^2S modestly increases. The LSSM spectroscopic factor of this isomeric state with the ground state of ^{132}Ba is $C^2S = 0.60$, which is large enough to support the proton $h_{11/2}$ configuration.

To discuss the intrinsic shape of the $11/2^-$ state of ^{133}La in terms of the shell-model framework, we show the energy surface and the T plot of the Monte Carlo shell-model (MCSM) calculations [55] in Fig. 6. In the figure the contour lines represent the energy surface obtained by the quadrupole-constrained Hartree-Fock method with the variation after parity projection [56] utilizing the same shell-model Hamiltonian. It shows the prolate minimum with modest triaxiality at $Q_0 = 260$ fm^2, which corresponds to the deformation parameter $\beta = 0.16$ using the potential energy surface of Fig. 6 through the relation suggested in Ref. [57]. The LSSM value

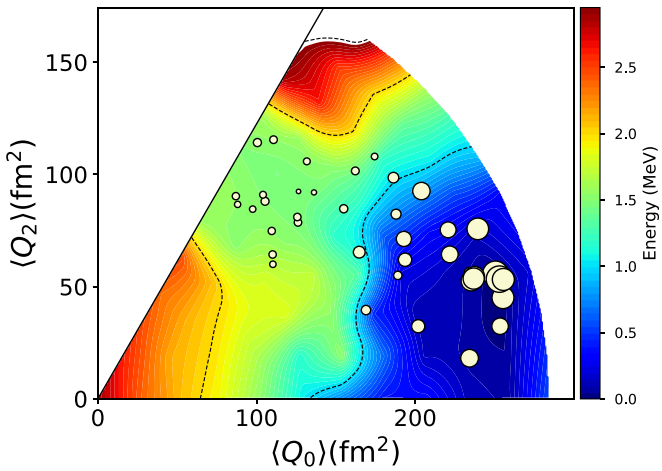

FIG. 6. T plot of the $11/2^-_1$ state in ^{133}La coordinated by the intrinsic mass quadrupole moments, Q_0 and Q_2. The contour line shows the energy surface obtained by the Q-constrained Hartree-Fock method with the variation after parity projection. The locations of the circles indicate the intrinsic shape of the MCSM basis states. The size of each circle denotes the overlap probability of the MCSM basis state and the total wave function, namely its importance in the total wave function.

of $Q = -1.25$ b provides the $\beta = 0.19$ by using Eq. (5), assuming $K = 1/2$.

In the MCSM framework, the resultant wave function is expressed as a superposition of the angular-momentum-projected, parity-projected Slater determinants, each of which is called an MCSM basis state. The intrinsic quadrupole deformation and its fluctuation are visualized utilizing the intrinsic quadrupole moments and the importance of these basis states. For visualizing the intrinsic deformation of the MCSM wave function, the quadrupole deformation of each MCSM basis state is represented as the position a white circle in Fig. 6, while its area denotes the overlap between the MCSM basis state and the resultant wave function, namely importance of the basis state. Such a figure is called a T plot. The MCSM basis states distribute around the minimum of the energy surface, indicating that the shell-model wave function of the $11/2^-_1$ state is a prolate shape with a certain shape fluctuation in the γ direction.

IV. CONCLUSION

In summary, the g factor and spectroscopic quadrupole moment measurement for the 535-keV isomer in ^{133}La has been carried out using TDPAD method The measured g-factor value for this isomer has been found to be 1.16 ± 0.07, along with the spectroscopic quadrupole moment $|Q| = 1.71 \pm 0.34$ b. Large-scale shell-model calculations have been performed to calculate the level structure of ^{133}La as well as to understand the configuration of the measured isomer at 535 keV excitation energy. The shell-model results provide an excellent description of the measured level scheme. In particular, the shell-model result on the g factor of the $11/2^-$ isomer, 1.16, matches the measured g factor of 1.16 ± 0.07 very well. The g factor provides the dominant configuration of $11/2^-$ isomeric state ^{133}La as $\pi(h_{11/2}) \otimes {}^{132}\mathrm{Ba}(0^+)$ by the LSSM study. The configuration is compatible with the coupling scheme of the odd mass La nuclei for the decoupled band built on $11/2^-_1$ state. For the quadrupole moment, shell-model calculation gives $Q = -1.25$ b, and $\beta = 0.19$ with assuming $K = 1/2$. The theoretical LSSM value of quadrupole moment is smaller than the measured one obtained from the combined interaction. A measurement of the pure quadrupole moment will be very helpful to understand the difference between theoretical and experimental values of this quantity.

ACKNOWLEDGMENTS

The authors acknowledge the TIFR-BARC Pelletron Linac Facility for providing good quality beam. The help and cooperation from S. M. Davane, B. Naidu, S. Jadhav, and R. Donthi for setting up the experimental apparatus is acknowledged. The authors thank JoAnn Totans, for her help to get old papers on ^{133}La. This work is supported by Department of Atomic Energy, Government of India (Project Identification Code: 12-R&D-TFR-5.02-0200), the International Joint Research Promotion Program of Osaka University, and the U.S. National Science Foundation (Grant No. PHY-1713857). R.P., N.S., Y.U., and E.I. acknowledge the RCNP Collaboration Research

network (COREnet) program. E.I. acknowledges KAKENHI grant (17H02893). N.S. and Y.U. acknowledge the priority issue 9 to be tackled by using Post K Computer (hp190160, hp180179), Interdisciplinary Computational Science Program in CCS, University of Tsukuba (xg18i035), KAKENHI grant (17K05433,15K05094).

[1] L. Kaya, A. Vogt, P. Reiter, M. Siciliano, B. Birkenbach, A. Blazhev, L. Coraggio, E. Teruya, N. Yoshinaga, K. Higashiyama, K. Arnswald, D. Bazzacco, A. Bracco, B. Bruyneel, L. Corradi, F. C. L. Crespi, G. de Angelis, J. Eberth, E. Farnea, E. Fioretto, C. Fransen, B. Fu, A. Gadea, A. Gargano, A. Giaz, A. Görgen, A. Gottardo, K. Hadyńska-Klęk, H. Hess, R. Hetzenegger, R. Hirsch, N. Itaco, P. R. John, J. Jolie, A. Jungclaus, W. Korten, S. Leoni, L. Lewandowski, S. Lunardi, R. Menegazzo, D. Mengoni, C. Michelagnoli, T. Mijatović, G. Montagnoli, D. Montanari, C. Müller-Gatermann, D. Napoli, Zs. Podolyák, G. Pollarolo, A. Pullia, M. Queiser, F. Recchia, D. Rosiak, N. Saed-Samii, E. Şahin, F. Scarlassara, D. Schneiders, M. Seidlitz, B. Siebeck, J. F. Smith, P.-A. Söderström, A. M. Stefanini, T. Steinbach, O. Stezowski, S. Szilner, B. Szpak, C. Ur, J. J. Valiente-Dobón, K. Wolf, and K. O. Zell, Phys. Rev. C **98**, 014309 (2018).

[2] S. Biswas, R. Palit, J. Sethi, S. Saha, A. Raghav, U. Garg, Md. S. R. Laskar, F. S. Babra, Z. Naik, S. Sharma, A. Y. Deo, V. V. Parkar, B. S. Naidu, R. Donthi, S. Jadhav, H. C. Jain, P. K. Joshi, S. Sihotra, S. Kumar, D. Mehta, G. Mukherjee, A. Goswami, and P. C. Srivastava, Phys. Rev. C **95**, 064320 (2017).

[3] H. Nishibata, R. Leguillon, A. Odahara, T. Shimoda, C. M. Petrache, Y. Ito, J. Takatsu, K. Tajiri, N. Hamatani, R. Yokoyama, E. Ideguchi, H. Watanabe, Y. Wakabayashi, K. Yoshinaga, T. Suzuki, S. Nishimura, D. Beaumel, G. Lehaut, D. Guinet, P. Desesquelles, D. Curien, K. Higashiyama, and N. Yoshinaga, Phys. Rev. C **91**, 054305 (2015).

[4] N. Shimizu, T. Mizusaki, T. Utsuno, and Y. Tsunoda, Comput. Phys. Commun. **244**, 372 (2019).

[5] R. Leguillon, H. Nishibata, Y. Ito, C. M. Petrache, A. Odahara, T. Shimoda, N. Hamatani, K. Tajiri, J. Takatsu, R. Yokoyama, E. Ideguchi, H. Watanabe, Y. Wakabayashi, K. Yoshinaga, T. Suzuki, S. Nishimura, D. Beaumel, G. Lehaut, D. Guinet, P. Desesquelles, D. Curien, A. Astier, T. Konstantinopoulos, and T. Zerrouki, Phys. Rev. C **88**, 044309 (2013).

[6] Md. S. R. Laskar, S. Saha, R. Palit, S. N. Mishra, N. Shimizu, Y. Utsuno, E. Ideguchi, Z. Naik, F. S. Babra, S. Biswas, S. Kumar, S. K. Mohanta, C. S. Palshetkar, P. Singh, and P. C. Srivastava, Phys. Rev. C **99**, 014308 (2019).

[7] M. Budzynsky, V. S. Buttsev, K. Y. Gromov, R. Ion-Mikhai, V. G. Kalinnikov, N. Z. Marupov, V. A. Morozov, T. M. Muminov, I. Kholbaev, and M. Yakhim, Yad. Fiz. **21**, 913 (1975) [Sov. J. Nucl. Phys. **21**, 469 (1976)].

[8] L. Hildingson, W. Klamra, Th. Lindblad, C. G. Lindén, G. Sietten, and G. Székely, Z. Phys. A **338**, 125 (1991).

[9] C. M. Petrache, and Q. B. Chen, and S. Guo, and A. D. Ayangeakaa, and U. Garg, and J. T. Matta, and B. K. Nayak, and D. Patel, J. Meng, M. P. Carpenter, and C. J. Chiara, and R. V. F. Janssens, and F. G. Kondev, T. Lauritsen, D. Seweryniak, S. Zhu, S. S. Ghugre, and R. Palit, Phys. Rev. C **94**, 064309 (2016).

[10] S. Biswas *et al.*, Eur. Phys. J. A **55**, 159 (2019).

[11] C. Gerschel, J. P. Husson, N. Perrin, and L. Valentin, International Conference on Properties of Nuclear States, Montreal, Canada (1969), p. 85.

[12] N. J. Stone, At. Data Nucl. Data Tables **90**, 75 (2005).

[13] M. Budzynski, M. Enikova, G. Lizurei, K. M. Muminov, A. I. Muminov, M. Subotovich, T. Khazratov, N. K. Chang, and Yu. V. Yushkevich, Program and Theses, Proc. 29th Ann. Conf. Nucl. Spectrosc. Struct. At. Nuclei, Riga (1979), p. 81.

[14] C. Gerschel *et al.*, Phys. Lett. B **33**, 299 (1970).

[15] B. Klemme *et al.*, Phys. Lett. B **45**, 38 (1973).

[16] F. S. Stephens, R. M. Diamond, J. R. Leigh, T. Kammuri, and K. Nakai, Phys. Rev. Lett. **29**, 438 (1972).

[17] J. R. Leigh, K. Nakai, K. H. Maier, F. Pühlhofer, F. S. Stephens, and R. M. Diamond, Nucl. Phys. A **213**, 1 (1973).

[18] K. Nakai, P. Kleinheinz, J. R. Leigh, K. H. Maier, and F. A. Stephens, R. M. Diamond, and G. Løvhøiden, Phys. Lett. B **44**, 443 (1973).

[19] M. S. Dewey, H.-E. Mahnke, P. Chowdhury, U. Garg, T. P. Sjoreen, and D. B. Fossan, Phys. Rev. C **18**, 2061 (1978).

[20] H. Ejiri, T. Shibata, and M. Takeda, Nucl. Phys. A **221**, 211 (1974).

[21] J. F. Ziegler, M. D. Ziegler, and J. P. Biersack, Nucl. Instrum. Methods Phys. Res. B **268**, 1818 (2010).

[22] SRIM-2013 manual and code available from: http://www.SRIM.org.

[23] S. N. Mishra, S. K. Mohanta, S. M. Davane, N. Kulkarni, and P. Ayyub, Phys. Rev. Lett. **105**, 147203 (2010).

[24] S. K. Mohanta, S. N. Mishra, K. K. Iyer, and E. V. Sampathkumaran, Phys. Rev. B **87**, 125125 (2013).

[25] S. Saha, S. K. Mohanta, Sayani Biswas, R. Palit, and S. N. Mishra, Hyperfine Interact. **237**, 121 (2016).

[26] H. E. Mahnke, Hyperfine Interact. **49**, 77 (1989); D. Reigel, K. D. Gross, E. Recknagal, and J. C. Soares, *Nuclear Physics Applications in Material Science*, Vol. E14407 of NATO Advanced studies Institute, Series B; Physics (Plenum, New York, 1988), p. 327.

[27] G. Schatz and A. Weidinger, *Nuclear Condensed Matter Physics* (Wiley, New York, 1996).

[28] E. B. Karlsson, *Solid State Phenomena: As Seen by Muons, Protons and Excited Nuclei* (Clarendon, Oxford, 1995).

[29] V. V. Krishnamurthy, S. Habenicht, K.-P. Lieb, M. Uhrmacher, and K. Winzer, Phys. Rev. B **56**, 355 (1997).

[30] S. N. Mishra, J. Phys.: Condens. Matter **21**, 115601 (2009).

[31] K. Alder and R. M. Steffen, Phys. Rev. **129**, 1199 (1963).

[32] H. Haas, Phys. Scr. **11**, 221 (1975).

[33] H. Frauenfelder and R. M. Steffen, Angular correlations, in *Alpha-, Beta-and Gamma-Ray Spectroscopy*, Vol. 2, edited by K. Siegbahn (North-Holland, Amsterdam, 1965), p. 997.

[34] L. Boström, E. Karlsson, and S. Zetterlund, Phys. Scr. **2**, 65 (1970).

[35] Md. S. R. Laskar *et al.*, Hyperfine Interact. **240**, 96 (2019).

[36] W. Witthuhn and W. Engel, in *Hyperfine Interactions of Radioactive Nuclei*, edited by J. Christiansen, Topics in Current Phys., Vol. 31 (Springer, Berlin, 1983), p. 205.

[37] P. Hohenberg and W. Kohn, Phys. Rev. **136**, B864 (1964).

[38] W. Kohn, and L. J. Sham, Phys. Rev. **140**, A1133 (1965).

[39] S. Cottenier, Density Functional Theory and the family of (L)APW-methods: A step-by-stem introduction (Instituut voor Kern-en Stralingsfysica, K. U. Leuven, Belgium) (freely available at http://susi.theochem.tuwien.ac.at/reg_user/textbooks/DFT_and_LAPW_2nd.pdf).
[40] E. Sjöstedt, L. Nordström, and D. J. Singh, Solid State Commun. **114**, 15 (2000).
[41] G. K. H. Madsen, P. Blaha, K. Schwarz, E. Sjöstedt, and L. Nordström, Phys. Rev. B **64**, 195134 (2001).
[42] P. Blaha, K. Schwarz, G. K. H. Madsen, D. Kvasnicka, and J. Luitz, *WIEN2k: An Augmented Plane Wave+Local Orbitals Program for Calculating Crystal Properties* (Karlheinz Schwarz, Technische Universität, Wien, 2001) (https://wiki.cse.ucdavis.edu/_media/support:hpc:software:wien2k_usersguide.pdf).
[43] P. Cherin and P. Unger, Acta Crystallogr. **23**, 670 (1967).
[44] J. P. Perdew, K. Burke, and M. Ernzerhof, Phys. Rev. Lett. **77**, 3865 (1996).
[45] S. N. Ghoshal, *Nuclear Physics* (S. Chand and Company Limited, New Delhi, 2018).
[46] L. Errico, K. Lejaeghere, J. Runco, S. N. Mishra, M. Rentería, and S. Cottenier, J. Phys. Chem. C **120**, 23111 (2016).
[47] M. Honma, T. Otsuka, T. Mizusaki, and M. Hjorth-Jensen, RIKEN Accelerator Progress Report **45**, 35 (2011).
[48] M. Honma, T. Otsuka, T. Mizusaki, and M. Hjorth-Jensen, RIKEN Accelerator Progress Report **49**, 77 (2015).
[49] T. Otsuka, T. Suzuki, M. Honma, Y. Utsuno, N. Tsunoda, K. Tsukiyama, and M. Hjorth-Jensen, Phys. Rev. Lett. **104**, 012501 (2010).
[50] L. Kaya *et al.*, Phys. Rev. C **100**, 024323 (2019).
[51] Y. Utsuno, T. Otsuka, N. Shimizu, M. Honma, T. Mizusaki, Y. Tsunoda, and T. Abe, EPJ Web Conf. **66**, 02106 (2014).
[52] J. Chiba, R. Hayano, M. Sekimoto, H. Nakayama, and K. Nakai, J. Phys. Soc. Jpn. **43**, 1109 (1977).
[53] P. Ring and P. Schuck, *The Nuclear Many-Body Problem* (Springer-Verlag, New York, 1980).
[54] Evaluated Nuclear Structure Data File (ENSDF).
[55] N. Shimizu *et al.*, Phys. Scr. **92**, 063001 (2017).
[56] T. Togashi, N. Shimizu, Y. Utsuno, T. Otsuka, and M. Honma, Phys. Rev. C **91**, 024320 (2015).
[57] Y. Utsuno, N. Shimizu, T. Otsuka, T. Yoshida, and Y. Tsunoda, Phys. Rev. Lett. **114**, 032501 (2015).